Reinforced Wool Keratin Fibers via Dithiol Chain Re-bonding

Jin Zhu, Ning Ma, Shuo Li, Liang Zhang, Xiaoling Tong, Yanyan Shao, Chao Shen, Yeye Wen, Muqiang Jian,* Yuanlong Shao,* and Jin Zhang*

Regenerated wool keratin fibers (RWKFs) have heretofore attracted tremendous interest according to environmental friendliness, ample resource, and intrinsic biocompatibility for broad applications. In this realm, both uncontrollable keratin fibril assembly procedure and resultant insufficient mechanical strength, have greatly hindered their large-scale manufacture and commercial viability. Herein, a continuous wet-spinning strategy is put forward to rebuild wool keratin into compact regenerated bio-fibers with improved strength via disulfide re-bonding. Dithiothreitol (DTT) has been introduced to renovate disulfide linkage inside keratin polypeptide chains, and bridge keratin fibrils via covalent thiol bonding to form a continuous backbone as mechanical support. A thus-derived RWKF manifests a tensile strength of 186.1 ± 7.0 MPa and Young's modulus of 7.4 ± 0.2 GPa, which exceeds those of natural wool, feathers, and regenerated wool or feather keratin fibers. The detailed wet-spinning technical parameters, such as coagulation, oxidation, and post-treatment, have been systematically optimized to guarantee the continuous preparation of high-strength regenerated keratin fibers. This work offers insight into solving the concurrent challenges for continuous manufacture of regenerated protein fibers and sustainability concerns about biomass waste.

1. Introduction

With the concerns of plastic pollution and global quest for sustainability, regenerated fiber materials produced from bio-mass resources, such as bamboo, straw, silk, feather, and wool, have received extensive attention to replacing petroleum-based synthetic fibers.[1–6] Reconstruction of bio-fibers through green processing technology even from waste bio-resources or textiles could not only significantly decrease environmental pollution, but also maintain their intrinsic biocompatibility and introduce unique functionalities via hierarchical structure design.[7–10] As a representative elementary building unit for a majority of bio-resources, keratin demonstrates prominent features for manufacturing high-strength bio-regenerated fiber, which is beneficial from its fibril nanostructure and ample source (wool, feather, horns, hooves, and even waste textiles).[11–14] By virtue of its robust mechanical properties, remarkable moisture transmission, and thermal preservation capability, wool has been widely used in textile industry, with an annual output exceeding 1.76 million tons worldwide.[15] Simultaneously, amount of wool waste is produced from the slaughterhouse, textile industry leftovers, and discarded fabrics/clothes globally every year.[16–18] Generally, a major amount of wool waste has been converted into low-value products, such as feed additives, cosmetic ingredients, or sewage treatment agents.[19–22] However, considering the wool ≈90% pure keratin content, crude/waste wool could serve as a valuable resource to regenerate biodegradable wool keratin into high-value-added bio-fibers.[23,24]

Wool keratin exhibits a complex hierarchical structure with nano-scale ordered fibrillar crystals embedded in the amorphous keratin matrix.[25,26] α- and β-keratin are two dominant

J. Zhu, N. Ma, L. Zhang, Y. Shao, C. Shen, Y. Wen,
M. Jian, Y. Shao, J. Zhang
Beijing Graphene Institute (BGI)
Beijing 100095, P. R. China
E-mail: jianmq@bgi-graphene.com; shaoyuanlong@pku.edu.cn;
jinzhang@pku.edu.cn
S. Li, L. Zhang, X. Tong, Y. Shao
College of Energy Soochow Institute for Energy and Materials
Innovations (SIEMIS)
Key Laboratory of Advanced Carbon Materials and Wearable Energy
Technologies of Jiangsu Province
Soochow University
Suzhou 215006, P. R. China

Y. Wen, J. Zhang
Center for Nanochemistry
Beijing Science and Engineering Center for Nanocarbons
Beijing National Laboratory for Molecular Sciences
College of Chemistry and Molecular Engineering
Peking University
Beijing 100871, P. R. China
Y. Shao, J. Zhang
School of Materials Science and Engineering
Peking University
Beijing 100871, P. R. China

filaments for constituting fine filament-matrix structures at nanoscale. The helical structure of α-keratin is stabilized by hydrogen bonds inside and between keratin chains, in which the twisted chain endows α-keratin with the prominent elastic mechanical feature. For β-keratin, the rigid pleated sheet consists of laterally packed β-strands, which are held together by disulfide bonds and cysteine-rich polypeptide chains crosslinking.[27,28] The disulfide intermolecular crosslinking is just like "mortar" to bridge the building wool keratin fibrils into an integrated bio-fiber.[29] In addition, the arrangement orientation and aggregate compaction also play a critical role in determining the final mechanical strength of regenerated fiber.[30] Although sufficient research efforts have been dedicated to producing wool keratin fiber even since 1940s, it's still a great challenge to efficiently recover disulfide crosslinking while forms into a compact and highly aligned wool keratin fibril arrangement for manufacturing tough regenerated fibers.[31,32] In order to improve the spinnability of keratin solution, wool keratin is blended with high molecular polymers such as viscose, polyvinyl alcohol (PVA), and hydroxypropyl methylcellulose.[33] However, compared to natural wool, the final fiber suffers from low keratin content (13-46 wt. %), poor mechanical properties, and greatly impaired fiber biocompatibility.[34,35] Benefiting from the tough tensile strength of β-keratin fibril, the mechanical strength of regenerated fibers prepared from β-keratin dominated poultry feathers was significantly improved to 160.7 ± 12.3 MPa.[36] Therefore, it remains a challenge to fabricate tough regenerated fibers from wool keratin to satisfy its mechanical requirement of yarn manufacturing and further weaving for broad applications.

Generally, re-bonding the keratin chain to extend the fibrils could be an efficient approach to reinforce regenerated keratin fibers. Herein, dithiothreitol (DTT) has been introduced in a wet spinning procedure to renovate the disulfide bonds in the keratin polypeptide chain, which can covalently re-bond the free sulfhydryl groups to introduce long-distance cross-linking. In addition, the drafting treatment triggered a highly ordered hierarchical structure and enhanced crystallinity significantly enhanced the tensile strength. The thus-fabricated regenerated wool keratin fiber (RWKF) manifests a tensile strength of 186.1 ± 7.0 MPa and Young's modulus of 7.4 ± 0.2 GPa, which far surpass natural wool and previously reported keratin-dominated regenerated fibers. Such a wool keratin fiber assembly strategy could offer a promising approach to rebuild protein waste toward constructing biocompatible fiber for textile or even biomedicine applications.

2. Results and Discussions

2.1. Wet-Spinning Preparation of RWKFs

Benefiting from its fascinating compatibility with current large-scale fiber production line, wet-spinning has been recognized as a promising strategy to continuously produce regenerated fibers.[37,38] **Figure 1**a schematically illustrates the wool keratin dispersion dope preparation and wet-spinning process. With this integrated approach, the extracted wool keratin has been reconstructed into highly compact and well-aligned regenerated

fibers with desirable mechanical strength and silk-like toughness via a disulfide re-bonding strategy. We utilize the waste coarse wool as the source to extract keratin fibrils for further wet-spinning dispersion dope. Although the deserted coarse wool presents a rough surface and thick diameter, which could not be directly used as high-grade wool fiber for further woolen sweater manufacturing, the chemical structure is consistent even with cashmere for extracting high-quality keratin fibril to assemble RWKFs. The physicochemical property of the waste coarse wool fiber has been characterized through scanning electron microscopy (SEM), X-ray diffraction (XRD), Fourier transform infrared spectroscopy (FTIR), and Raman spectra. The raw fiber exhibits a diameter of 44.5 um and tensile strength of 97.4 ± 16.6 MPa, with a majority content of α-helix keratin fibril (Figure S1, Supporting Information).

Generally, the keratin fibril is connected via disulfide covalently bonding to form the final hierarchical microfibril and microfilament structures.[39,40] As shown in Table S1 (Supporting Information), we compare the different keratin extraction methods and find our optimized method offers an extremely high keratin extraction rate. To extract keratin fibril, cysteine, urea, and sodium dodecyl (SDS) has been utilized to solubilize coarse wool by destroying the disulfide network and simultaneously eliminating sulfhydryl moieties. Then keratin powder is collected after a series of sequential procedures, such as filtration, salting out, and freeze-drying (Figure S2a, Supporting Information). Additionally, from the perspective of practical application, this method can be extended to other types of waste wool, such as fine wool and fallen wool from yarn manufacture (Figure S3, Supporting Information). FTIR spectroscopy and XRD in Figure S2 (Supporting Information) have been conducted to analyze the physicochemical structure with comparison of original coarse wool. The thus-derived keratin powder manifests the representative amide I ($1700–1600$ cm^{-1}), amide II ($1600–1500$ cm^{-1}), and amide III ($1350–1200$ cm^{-1}) peaks in Figure S2c (Supporting Information), which is in great coincident with the essential structure of natural wool. It indicates that the extracted keratin powder greatly maintains the intrinsic wool keratin structure. In addition, thermogravimetric analysis (TGA) also presents that the extracted keratin powder demonstrates similar thermal stability to the original coarse wool.

Reestablishing the hierarchical filament structure via re-bonding wool keratin fibril is the crucial process to fabricating the high-strength RWKFs. We pioneeringly introduce the dithiothreitol (DTT) in the wet-spinning dispersion with Na$_2$CO$_3$/NaHCO$_3$ aqueous solution to further cleave disulfide bonds to produce a highly concentrated keratin dispersion (Figure S4, Supporting Information). The high-viscosity keratin dope was extruded from a spinneret and introduced into the acetic acid/ethyl alcohol coagulation to drive the RWKF solidification and orderly assembly. During this procedure, DTT enables the restoration of the intramolecular and intermolecular disulfide covalent network by the hydrogen peroxide (H$_2$O$_2$) oxidation on the sulfhydryl groups[9] to guarantee the compact structure of the thus-fabricated RWKFs. As exhibited in Figure 1b, we collected ≈5000 meters long RWKF after a continuous wet-spinning process within 7 hours, and the fabricated RWKF demonstrate silk-like luster.
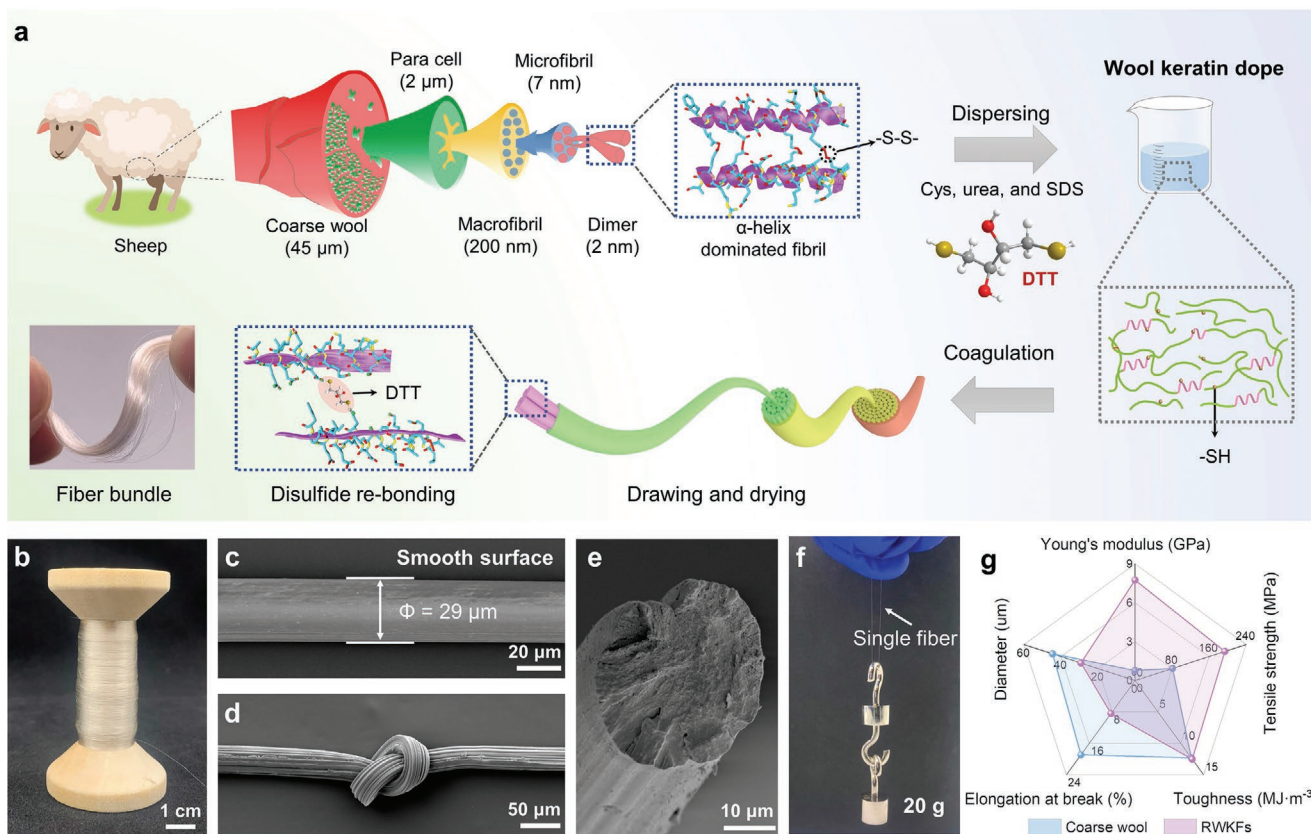
Figure 1. Continuous preparation of RWKFs by reconstituting the disulfide bridges. a) Schematic diagram showing the hierarchical structure of wool fibers, the extraction process of keratin protein, and the wet spinning approach to continuously produce reinforced RWKF by disulfide re-bonding. b) Optical image of the as-spun continuous filament with a length of >5000 meters. c) SEM images for the surface morphology of RWKF. d) Knotted RWKF showing excellent flexibility. e) SEM images for the cross-section of wool keratin fiber. f) A single regenerated fiber (with a diameter of 36 µm) that lifts a 20 g weight, revealing its distinguishing mechanical strength. g) Performance comparison between the prepared RWKF and pristine coarse wool.

As exhibited in Figure 1c and Figure S5 (Supporting Information), the thus-fabricated RWKF exhibits a smooth surface morphology and uniform diameter of ≈29 µm, which is significantly different from scale epicuticular rough structure with a thicker diameter of 46.4 ± 2.3 µm and 33.4 ± 0.5 µm for natural wool (Figure S5a, Supporting Information) and degreased wool (Figure S5b, Supporting Information). The cross-sectional SEM image in Figure 1e indicates the dense-packing morphology without prominent voids. Figure 1d depicts that the RWKF could be simply tied tightly into a knot without destroying the elementary filament structure, which further verifies its flexibility and high tensile strength. In a result, a single RWKF could lift a 20 g weight without any other support, as indicated in Figure 1f. We summarize the mechanical properties of RWKF in comparison with coarse wool in Figure 1g, which indicates that RWKF manifests a 7.75 GPa Young's modulus and 12.5 MJ m^{-3} toughness in stark contrast to 0.78 GPa, 12.3 MJ m^{-3} for coarse wool. Simultaneously, the chemical structure of the RWKF has been also verified through XRD, FTIR, and Raman spectra. The XRD curve in Figure S6c (Supporting Information) conspicuously depicts annihilation of α-helix peak and strengthening of β-sheet peak intensity. It attributes to the efficient recapitulation of disulfide bonds network and rational construction of long-distance crosslinks,[35,36] thereby increasing the content of

β-sheet crystals and further yielding high-performance keratin fibers.

2.2. Regulation of Wet-Spinning Dope Rheologic Behavior via Inducing DTT

Wet-spinning dope rheologic behavior, i.e., viscoelasticity, is the crucial feature to determine the dispersion spinnability.[41] As demonstrated in Figures S7 and S8 (Supporting Information), the highly concentrated keratin (15-30 wt. %) manifests a jelly-like solid gel. In the range of shear rate 0.03-800 s^{-1}, the viscosity of keratin spinning solution increases with the increase of keratin content. Taking the shear rate of 0.1 s^{-1} as an example, the viscosity of the spinning fluid of 15–30 wt % is 613.8 Pa·s, 7524.8 Pa·s, 11 827.2 Pa·s, 34 316.8 Pa·s. Besides, when the amount of keratin added reaches 30 wt. %, partial undissolved keratin can be observed when the solution is supersaturated. While the low concentrated keratin presents a drop liquid feature, the viscosity of 5 and 10 wt.% keratin spinning dope at the shear rate of 0.1 s^{-1} is 0.007 and 3.9 Pa·s, respectively, which are far lower than these of high concentrated keratin dope. Such rheologic dispersion without any viscoelastic feature could not be processed into an intact filament through a wet-spinning
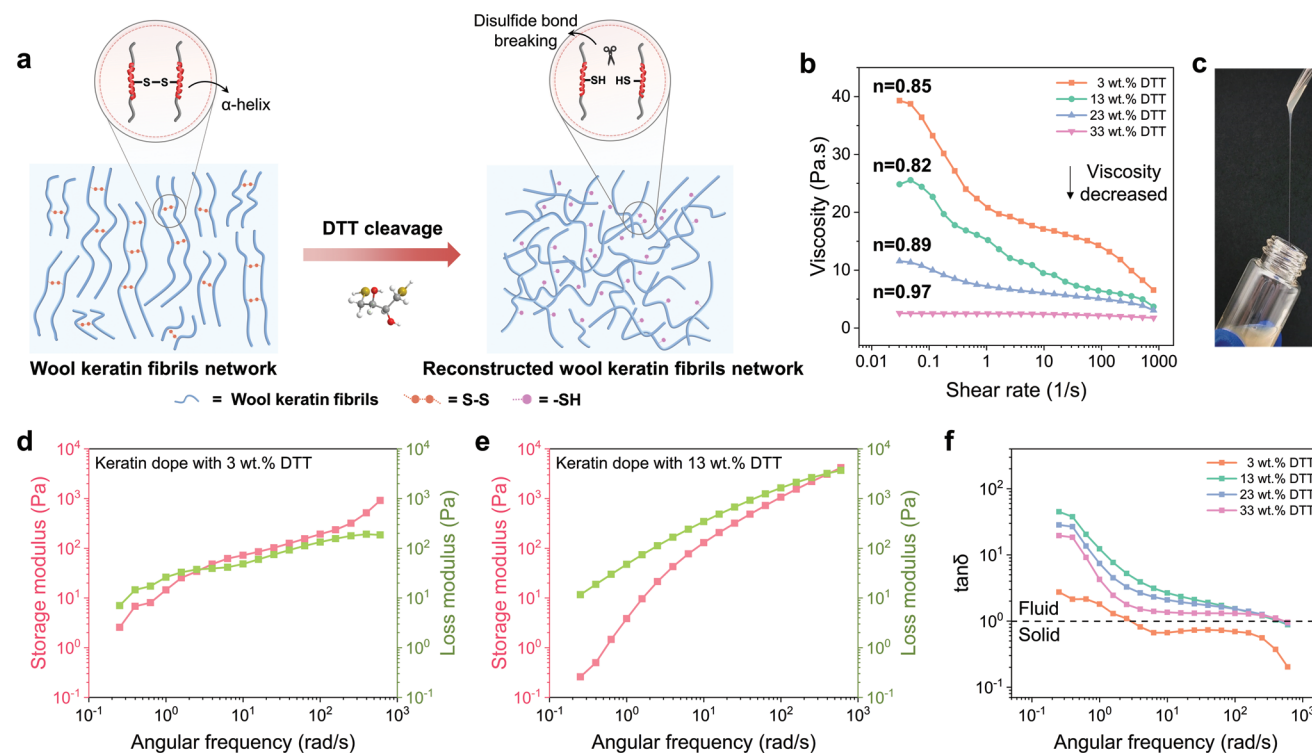
**ADVANCED
SCIENCE NEWS**

www.advancedsciencenews.com

**ADVANCED
FUNCTIONAL
MATERIALS**

www.afm-journal.de

Figure 2. DTT for controlled cleavage of disulfide bonds and tuning the rheological behavior of keratin spinning dopes. a) Schematic diagram of DTT cleaving the keratin disulfide bonds. b) Rheological properties of the keratin dope containing the as-extracted 25 wt. % protein, showing a decrease in viscosity with the increase in DTT and a shear-thinning behavior. c) Picture of fibers that are drawn directly from keratin dope that contains 13 wt. % DTT. The flow behavior index of the keratin dope. Storage modulus (G') and loss modulus (G'') of different keratin dopes containing d) 3 wt. %, e) 13 wt. % DTT. f) Measured rheological properties are $\tan\delta$ over variable angular frequency. $\tan\delta = G''/G'$, $\tan\delta$ indicates the viscoelasticity of the material. The critical strain at $\tan\delta = 1$ is the strain at rupture and can be used as a measure of ductility. When $\tan\delta > 1$, the material exhibits more viscous behavior.

strategy. As schematically illustrated in **Figure 2**a, DTT can efficiently cleave the disulfide bonds[9,35] by providing extra volume for keratin chain entanglement.

We optimize the DTT addition amount from 3 wt. % to 33 wt %, the cleavage of disulfide linkages gradually increases (Figure S9, Supporting Information). Similarly, it leads to a gradual decrease in the keratin molecular weight according to the rheology measurements of the keratin dope, showing an increase in viscosity and shear-thinning property upon DTT concentration increase, thereby resulting in protein solution viscosities decrease (Figure 2b). As the shear rate increased from 0.03 to 1000 s^{-1}, the viscosity of the DTT-regulated wet-spinning dope displays a gradual decline from 39.3 to 2.6 Pa·s, exhibiting an obvious shear-thinning behavior. The controlled disulfide bond cleavage could split the twisted keratin strand into long-chain forming into chain entanglement.[36] Therefore, DTT addition could efficiently tune the keratin dope rheological properties and produce a viscoelastic dispersion.

We used the stretching test to investigate the stretchability of the spinning dopes under extensional flow. As demonstrated in Figure S10 (Supporting Information), while viscosity gradually decrease according to the DTT cleavage of disulfide bonds, the keratin dope transformed from the quasi-solid state to viscoelastic phase, and finally to Newtonian fluid. With a 13 wt % DTT addition, the keratin dope demonstrates that the viscoelastic

dope could be formed simply by pulling the keratin dispersion with a lab spoon (Figure 2c). Afterward, we further systematically studied the flow behavior and dynamic rheological property of the keratin dope. Shear stress of keratin spinning dopes could be tested via a rotational rheometer for determination of consistency coefficient (K) and non-Newtonian exponent (n), according to the following equation (1):

$$\tau = K\gamma^{n-1} \tag{1}$$

where γ is the shear rate. In addition, the non-Newtonian exponent is a typical parameter to evaluate the molecular entanglement degree. The keratin dope with a lower value of n refers to the higher molecular entanglement, which tends to form into long-chain cross-linking with enhanced spinnability. As exhibited in Figure 2b, the keratin dope with 13 wt. % DTT manifests lowest n value of 0.82. This mainly attributes to the proper amount of DTT addition leading to the partial disulfide bonds cleavage for forming a uniform and stable keratin dispersion with an enhanced spinnability. As the increase of DTT ratio, the extra keratin fibrils have been cleaved via disulfide de-bonding, which leads to the gradual thinning of the keratin dope even reaching the Newtonian fluid (Figure S10, Supporting Information). The dynamic rheological properties of keratin dopes with different DTT addition ratios have been analyzed as shown in Figure 2d and Figure S11 (Supporting Information). Keratin dope dispersion with 3 wt. %

**ADVANCED
SCIENCE NEWS**

www.advancedsciencenews.com

**ADVANCED
FUNCTIONAL
MATERIALS**

www.afm-journal.de

DTT addition presents a higher storage modulus than the loss modulus while a shear rate above 2.5 rad s^{-1}, which indicates elasticity-dominated viscoelastic property. As a result, the protein molecular chains can hardly assemble into densified and aligned fibers subjected to the shear stress during a wet-spinning process.

In contrast, while the DTT content increased to 13 wt. %, the storage modulus of keratin spinning dope is lower than the loss modulus within a shear rate ranging from 0.1 to 600 rad s^{-1}, indicating that the protein solutions have a good viscosity for continuous wet-spinning (Figure 2e). To realize the continuous spinning fluid extruded from the wet-spinning spinneret, the spinning dope should form into a viscoelastic jetting fluid. The elastic type polymer chain is difficult to form thinning fluid, which is crucial for the wet-spinning dope stretching into high aspect ratio fiber. When tanδ (the ratio between viscosity and elasticity) is >1, the viscoelastic feature of the dispersion is viscous behavior dominated. The rheological measurements in Figure 2f and Figure S11 (Supporting Information) demonstrate that wet-spinning dope with 3 wt. % DTT addition is elastic feature dominated, while the spinning dope with DTT ratio from 13 wt. % to 33 wt. % is viscous behavior dominant. In addition, keratin dispersion with 13 wt. % DTT addition manifests the most prominent viscous dominant rheological behavior, which tends to form an ideal wet-spinning dope for continuous RWKF production.

2.3. Keratin Secondary Structure Reconstruction via Dithiol Chain-Extending

DTT addition has been verified to be an efficient strategy to enhance the mechanical property of wet-spun RWKF, after optimization of the ratio in keratin wet-spinning dope. However, the detailed mechanism for such remarkable improvement is still indistinct so far. As schematically illustrated in **Figure 3**a, we proposed that the unique dithiol structure enables DTT to play a chain-extending role in free sulfhydryl groups on keratin chains, which act as "bridges" to connect free sulfhydryl groups on cleaved keratin chains. The oxidative activity of 1% v/v hydrogen peroxide toward cysteine thiol groups conferred efficient covalent disulfide network recovery.[42] In addition, the length of the DTT molecular chain facilitates the collision of free sulfhydryl groups on different keratin chains, thereby promoting the efficient reconstruction of disulfide crosslinking.

To probe the detailed chemical structure evolution via DTT-involved keratin chain extension during the oxidation process, solid-state nuclear magnetic resonance (^{13}C NMR), and Raman spectroscopy have been conducted to characterize the detailed chemical and aggregate structure of coarse wool, unoxidized RWKFs, and oxidized RWKFs (Figure 3b,c). ^{13}C NMR confirmed the chain-extending effect of DTT on free sulfhydryl groups on keratin. As depicted in the ^{13}C NMR spectra, the characteristic peaks located at chemical shifts ≈54 ppm and
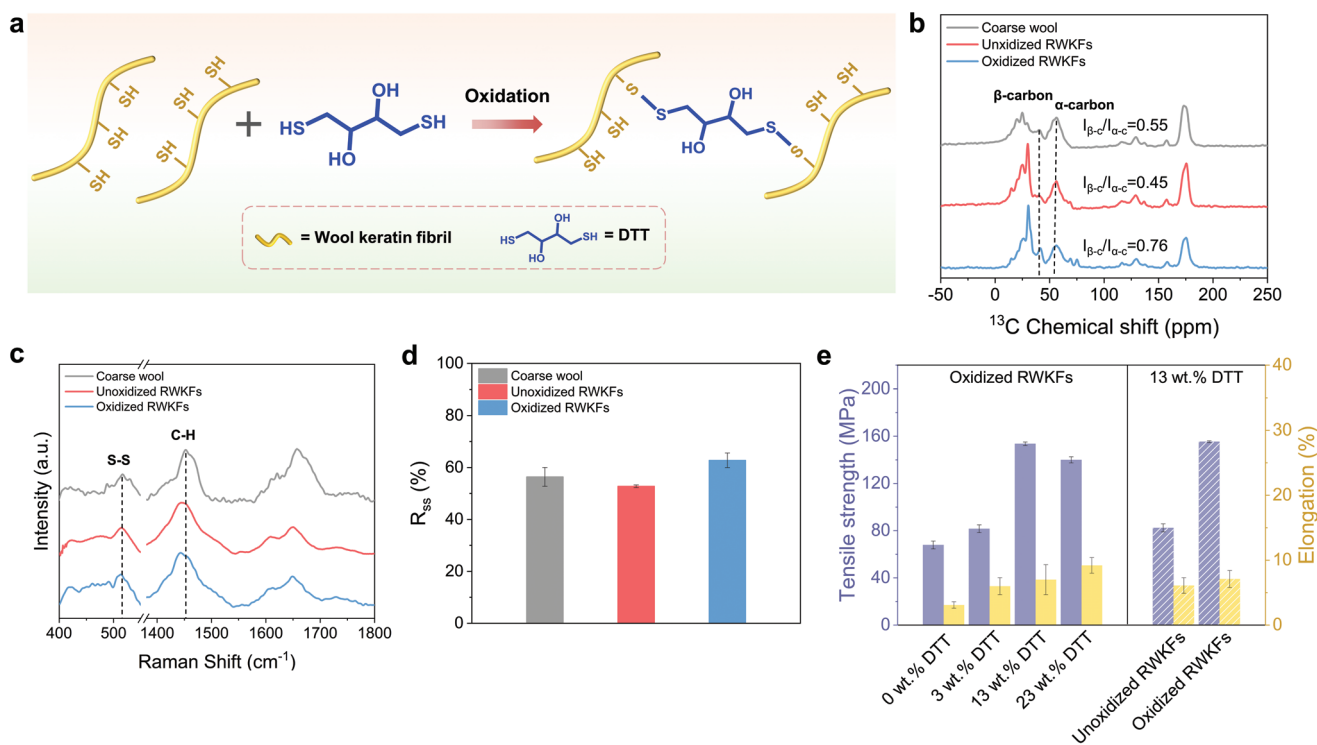

Figure 3. Schematic diagram of covalent cross-linking between DTT and keratin. a) Schematic diagram of covalent cross-linking between DTT and keratin. The free sulfhydryl groups of the keratin were re-oxidized to form disulfide bonds and DTT chain extension to reconstruct disulfide bonds. b) ^{13}C NMR spectra of coarse wool, unoxidized RWKFs, and oxidized RWKFs show that DTT molecules are bonded to the keratin backbone through covalent bonds. The ratio of β-carbon/α-carbon is the intensity of the peak at ≈40 ppm chemical shift divided by the intensity of the peak at ≈54 ppm chemical shift. c) Raman spectra analyzed the change of disulfide bond content in three kinds of fibers. DTT's dithiol structure and long molecular chain are beneficial to the binding of free sulfhydryl groups on keratin. d) R_{ss} is the ratio of peak areas of S-S band (500 cm^{-1}) and C—H band (1450 cm^{-1}). e) Comparison of changes in mechanical properties of fibers before and after oxidation.

**ADVANCED
SCIENCE NEWS**

www.advancedsciencenews.com

**ADVANCED
FUNCTIONAL
MATERIALS**

www.afm-journal.de

40 ppm were attributed to α-carbon and β-carbon in cysteine residues, respectively.[43–45] In a result, the β-carbon/α-carbon ratio of oxidized wool keratin fibers (0.76) demonstrated a dominant enhancement than that of unoxidized wool keratin fibers (0.45) and coarse wool (0.55). It verified that the β-sheet/α-helix secondary structure transformation was achieved during the DTT cleavage and subsequent oxidation reconstruction process (Figure 3b).[46]

Raman spectroscopy (Figure 3c) has been also put forward to characterize the secondary structure of keratin fibers, in which the disulfide content (R_{ss}) was extracted from the deconvolution of C—H band at 1450 cm^{-1}.[47,48] The normalization of Raman spectral data was based on the C—H band due to its large peak area and not affected by chemical treatment.[49,50] The disulfide bond content in fibers was calculated according to the following formula (2):

$$R_{ss} = \frac{S_{500}}{S_{1450}} \qquad (2)$$

where S_{500} is the peak area of S—S band (470-560 cm^{-1}), while S_{1450} is C—H band peak area (1430-1500 cm^{-1}). The disulfide bond contents of natural wool, unoxidized wool keratin fibers, and oxidized wool keratin fibers were calculated to be 56.4±3.6%, 52.8±0.5%, and 62.8±2.8%, respectively (Figure 3d). R_{ss} ratio increase indicates the effective recovery of disulfide crosslinking after DTT-induced cleavage and subsequent oxidation chain-extending. In addition, the dithiol structure also could form into disulfide bonding even between the parallel keratin fibrils to enhance the mechanical strength. Energy dispersive spectroscopy (EDS) has been also utilized to investigate the elemental distribution in coarse wool, keratin powder, and keratin fiber with/without DTT chain extension (Figure S12, Supporting Information). The resultant RWKF with dithiol-derived chain extension manifests an S element content of 87.8%, which is much >76.7% of keratin fiber without DTT decoration and the initially extracted keratin powder (61.1%). The S content variation further verifies the DTT-triggered disulfide bonding reconstruction. As presented in Figure 3e and Figure S13 (Supporting Information), we systematically characterized the mechanical strength of different DTT addition ratios from 0 wt. % to 23 wt. %. The tensile strength of the RWKF remarkedly increased from 67.9 MPa to 153.6 MPa, while the DTT addition increased from 0 wt. % to 13 wt. %. Simultaneously, the elongation also extends from 3.1% to 7%, which further confirms the mechanical strength improvement derived from the DTT-induced keratin chain extension. To further highlight the effect of oxidation-induced disulfide re-bonding construction, we also compared the mechanical property of the RWKF with/without the oxidation reconstruction step containing the consistent DTT ratio (Figure S14, Supporting Information). It demonstrated that the tensile strength significantly improved from 82.4 MPa to 155.4 MPa.

2.4. Drafting-Induced Rearrangement of the Secondary Structure of RWKFs

Drafting is a critical procedure for improving tensile strength via fibril orientation and filament densification. Inspired by

the traditional drafting engineering strategy, we apply the continuous stress on keratin fiber could efficiently maximize the secondary structure transition from α-helix to β-sheet, while significantly enhancing the fibril alignment.[9,51] It could enable the keratin fibrils to reassemble into a highly oriented and densely packed hierarchical structure, as illustrated in **Figure 4a**. Overall, nearly every step during the filament formation process involves drafting treatment. The morphology evolution in SEM images (Figure 4b) exhibited the diameter shrinking from 69.3 ± 0.57 μm to 29.2 ± 0.13 μm upon increasing the drawing ratio (λ) from 2.4 to 4.8. It should be noticed that once the drawing ratio exceeds 4.8, the keratin fibers are deformed into irregular shapes before they are fully solidified in the coagulation bath, which leads to anomalous fiber with coarse surface morphology and insufficient continuity (Figure S15, Supporting Information). Afterward, Raman spectra (Figure 4c) have been utilized to monitor the keratin secondary structure rearrangements.[9] We deconvoluted the typical peak assigned to amide I into α-helix (1652 cm^{-1}) and β-sheet (1671 cm^{-1}) keratin. The calculated β-sheet proportion significantly increased from 17.8% to 39.4%, while the drawing ratio raised from 2.4 to 4.8. FTIR spectra also have been conducted to analyze the secondary structure transition, which could be deconvoluted into three Gaussian peaks located at 1650 cm^{-1}, 1620 cm^{-1}, and 1670 cm^{-1} corresponding to α-helix, β-sheet and disordered structures (Figure S16, Supporting Information).[52,53] It also indicates the gradually increasing trend while aggrandizing the drawing ratio. The RWKF with 4.8 drawing ratio manifests a consistent β-sheet ratio of 39.5% with the Raman spectra result (Figure 4d).

In addition to the secondary structure transition, the crystalline ratio and nanofibril orientation also play a crucial role in determining the mechanical properties of the final resultant RWKFs. A series of X-ray techniques, such as 1D X-ray diffraction (XRD), 2D small-angle X-ray scattering (SAXS), and wide-angle X-ray scattering (WAXS) characterize the keratin molecular arrangement structure with varied drafting ratios. As summarized in Figure 4e,f and Figure S17 (Supporting Information), RWKF exhibits a significantly improved ordering degree, with orientation factor (f) increasing from 0.74 to 0.82. Meanwhile, WAXS and XRD have been also put forward to evaluate the crystallinity and crystalline orientation. It is well known that natural wool has two characteristic diffraction peaks, representing α-helix ($2\theta = 9°$) and β-sheet ($2\theta = 20°$) keratin fibrils.[54] As summarized in the 1D XRD pattern in Figure S18 and Table S2 (Supporting Information), the drafted RWKF exhibits suppressed features of α-helix and promoted crystallization.

Figure 4g shows the dependence of the tensile strength on the drawing ratio, showing a strong positive correlation between them (detailed mechanical properties are shown in Figure S19, Supporting Information). With the increase of drawing ratio from 2.4 to 4.8, the tensile strength of RWKFs increased from 144.9 ± 4.9 MPa to 186.1 ± 7.1 MPa, corresponding to an enhancement of ≈28.4%. It should be noted that although the DTT chain extension strategy and the high stretch ratio during spinning improve the tensile strength of RWKF, the stretching process consumed part of the deforming capacity of the keratin molecular chain, leading to the reduction of elongation at break. The average elongation at fracture
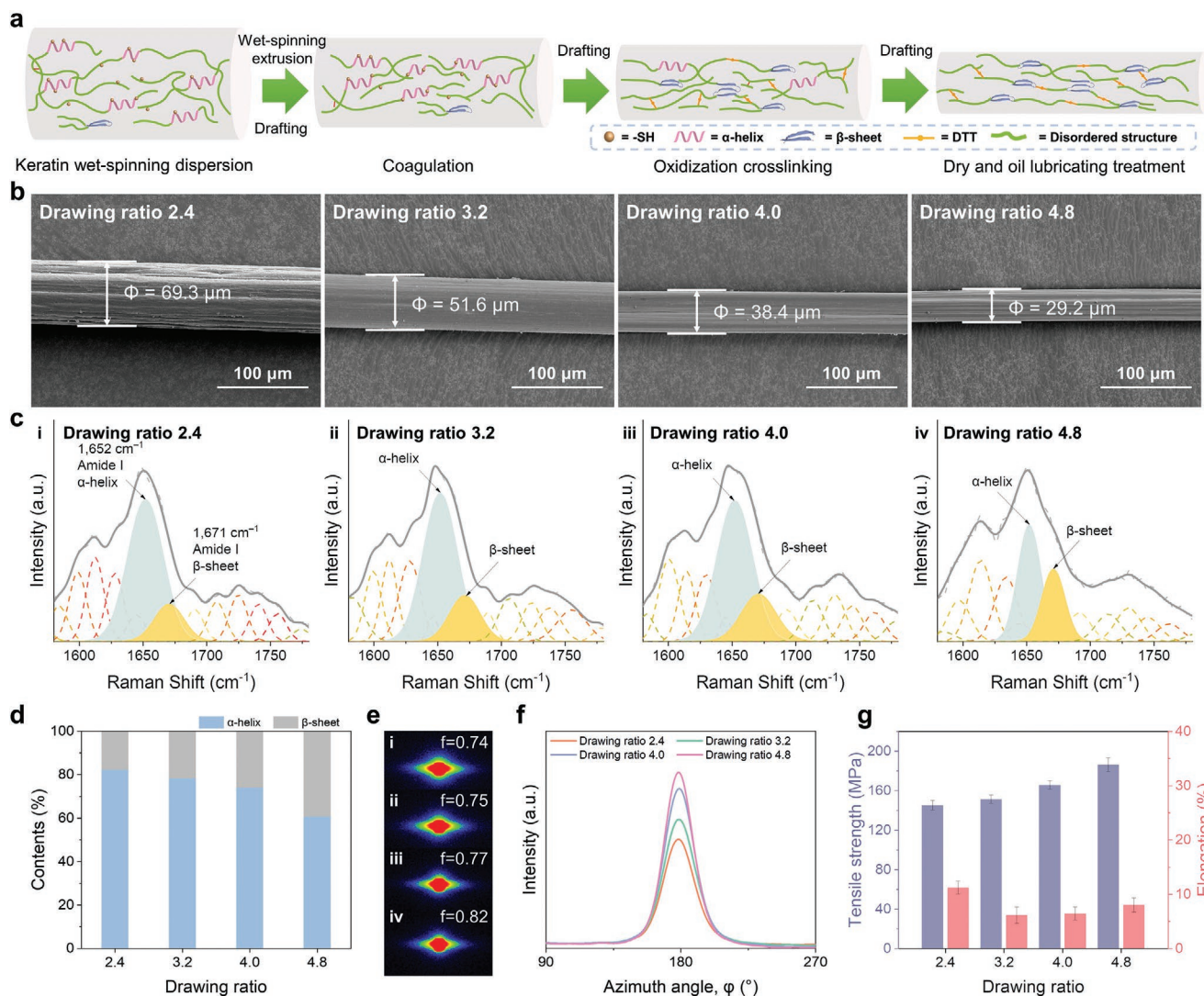
Figure 4. Drafting-induced rearrangement of the secondary structure of RWKFs a) Schematic diagram of keratin fiber structure changes during wet spinning. b) Microscopic morphological changes of keratin fibers characterized by SEM at different drawing ratios. c) Raman spectroscopy analysis of the structural transformation of single keratin fiber from α-helix to β-sheet under different drawing ratios. i–iv indicates that the drawing ratios are 2.4, 3.2, 4.0, and 4.8, respectively. The gray dotted line and the gray solid line represent the sum of the experimental peak and the calculated peak respectively. Similar results were obtained for $n = 3$ independent fiber samples. d) specific α-helix and β-sheet content ratios calculated from the Amide I Raman peak deconvolution. e) 2D SAXS profiles of keratin fibers with four different stretch ratios. i–iv indicates that the drawing ratios are 2.4, 3.2, 4.0, and 4.8, respectively. f) Azimuth (φ) plot of keratin fibers with four different stretch ratios prepared by the DTT chain extension strategy. The results confirmed that keratin fiber microfibrils were assembled into highly ordered structures by high stretching. g) Mechanical properties of keratin fiber under different drawing ratios.

slightly decreased from 11.2% at a drawing ratio of 2.4 to 8.0% at a drawing ratio of 4.8. However, due to the significant enhancement in Young's modulus and tensile strength, the toughness of the continuously drafted RWKF still improved significantly, with an average toughness of 10.9 ± 2.1 MJ m^{-3} for a 4.8 drawing ratio (Figure S20, Supporting Information).

2.5. Mechanical Properties and RWKF Textile Application

Although the structure of the primary protein fiber has been basically formed after oxidation and drafting, the time of the above process is shorter than the time needed for the movement

of the keratin macromolecular chain, so there are some internal stresses and defects in the fiber. Coating the resultant keratin fiber with a chemical agent (e.g., glycerol) via an oiling strategy could efficiently eliminate the electrostatic accumulation induced by the spinning and drafting process while maintaining the soft and smooth characteristics of the resultant fiber. In addition, the oiling procedure could efficiently improve the elongation at break, which is a key parameter for yarn manufacturing. In a result, successful commercial application of RWKF in textile industry requires that the elongation at break should be higher than 10%.[55] In this regard, glycerol has been selected as the chemical agent for oiling treatment. Glycerol is a typical hydrophilic additive agent, which could serve a great
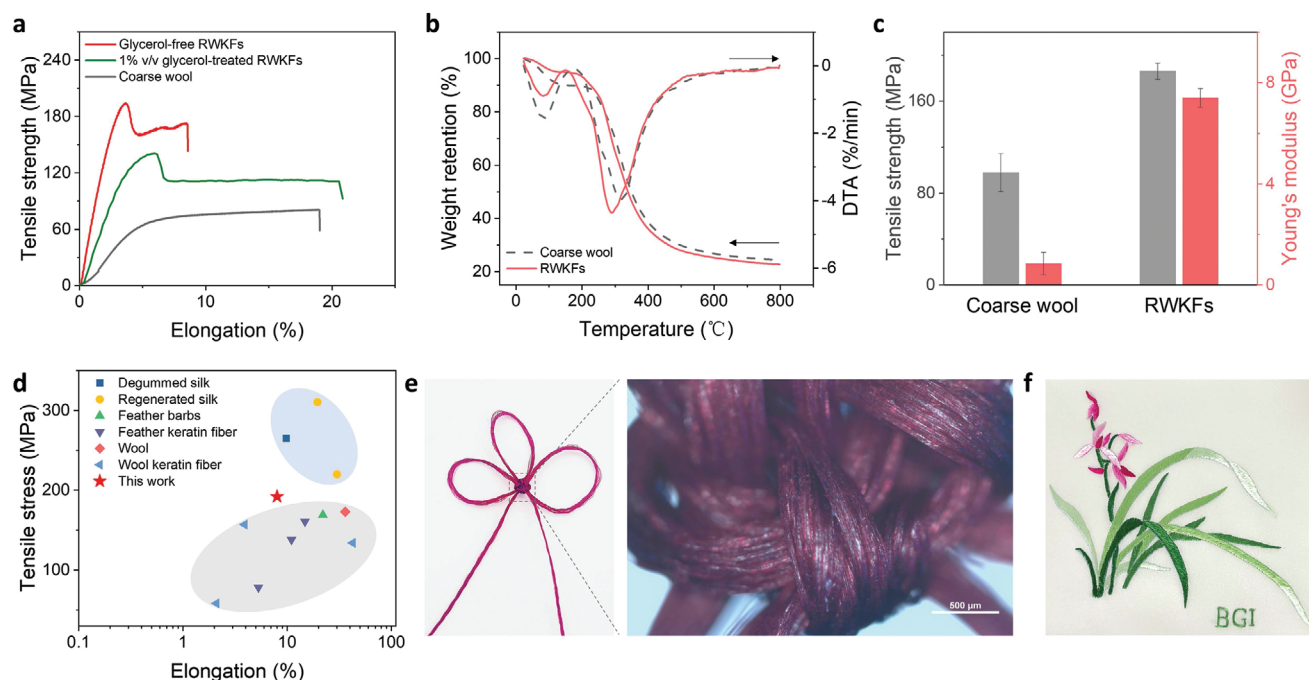
Figure 5. Mechanical properties and textile applications of keratin fibers. a) Typical stress-strain curves of coarse wool, glycerol-free RWKFs, and 1% glycerol-treated RWKFs. b) TGA and DTA curves of coarse wool and RWKFs. c) Comparison of tensile strength and Young's modulus of RWKFs (strength: 186.1 ± 7.1 MPa; modulus: 7.4 ± 0.37 GPa) and coarse wool (strength: 97.4 ± 16.6 MPa; modulus: 0.85 ± 0.44 GPa). d) Comparison of tensile strength of RWKFs with other natural fibers and regenerated keratin fibers. Detailed data and their sources are shown in Table S3 (Supporting Information). e) 24 keratin fibers were woven with sorrel knot, one of the Chinese knots. For image clarity, the keratin fibers were dyed with acid red B. f) Photograph of the embroidery display of keratin fibers after dyeing, which illustrates the textile application of the prepared RWKFs.

role in facilitating moisture adsorption in RWKF by weakening the interaction between keratin macromolecules. We treated the RWKF with 1% v/v glycerol, which improves the elongation at break to 20.6% while maintaining the tensile strength to 140.8 MPa. The elongation is approaching the natural wool (18.9%), but tensile strength is remarkably reinforced (81.1 MPa for natural wool). Thus, oiling post-treatment offers a great opportunity to optimize the surface structure of the resultant keratin fiber, providing a mechanical property balance between the tensile strength and elongation at break (**Figure 5a**; Figure S21, Supporting Information). Afterward, the thermal stability has been also characterized via thermogravimetric analysis (TGA) and differential thermal analysis (DTA) in Figure 5b. The resultant RWKF demonstrated a similar decomposition temperature at 240.2 °C in N_2 atmosphere, which is quite close to that of coarse wool with rigid scale layer protection.[54] Meanwhile, there was no significant difference in the degradation rate and weight loss rate between RWKF and natural wool, which can be attributed to the similar crystallinity of natural wool and the high degree of disulfide crosslinking of RWKF.

The high strength, toughness, and light weight of RWKF endows it with plenty of textile applications. Owing to its predominant mechanical properties of 186.1 ± 7.0 MPa tensile strength and Young's modulus of 7.4 ± 0.2 GPa (Figure 5c), the resultant RWKF offers promising potential in plenty of textile applications. As summarized in the curve in Figure 5d and Table S3 (Supporting Information), it is worth noting that the ultimate tensile strength of the current RWKF surpassed all that of natural wool, feathers, and previously reported

regenerated wool fibers and even regenerated feather protein fibers with higher β-sheet ratio.

In addition to mechanical properties, the dyeing and braiding properties of keratin fibers are also important for practical textile engineering applications of fibers. To this end, we perform a simple braiding to further evaluate its hooking performance. The high tensile strength and toughness allow the use of crochet hooks to crochet single fibers (Figure S22, Supporting Information). Here, a fiber bundle composed of 24 fibers was woven into a traditional Chinese knot. It was observed by optical microscopy that the fibers were bright and shiny, closely crossed in the meridional and zonal directions, without obvious cracks on the surface (Figure 5e). We further stained RWKF with acid dyes of different colors to assess the staining ability of the samples. Taking the acid yellow dye as an example, the dye uptake was 60.2%, which showed good dyeing ability (Figure S23, Supporting Information). The dyed fibers can be embroidered into brightly colored and beautifully patterned crafts (Figure 5f).

3. Conclusion

Overall, we have demonstrated a simple and effective continuous wet-spun preparation strategy for RWKFs to convert waste wool into high-strength regenerated keratin fibers. The superior mechanical properties are not only due to the introduction of long-distance cross-linking by DTT chain extension, but also beneficial from the transition from α-helical to

β-sheet structure induced by high-fold stretch during wet spinning, which facilitates efficient stress transfer. According to this unique structural design, the obtained RWKFs exhibited a tensile strength of 186.1 ± 7.0 MPa and Young's modulus of 7.4 ± 0.2 GPa, much higher than any other reported regenerated keratin fibers, and feathers, slightly higher than that of natural wool and even comparable to silk. The subsequent oiling, drying post-treatment and the significant dyeing capability, and thermal stability also remarkably demonstrate its potential in textile industry.

4. Experimental Section

Materials and Chemicals: The waste coarse wool was provided by Zhangjiagang Yangtse Dye Co., Ltd. L-cysteine (Cys), 1, 4-dithiothreitol (DTT), lithium bromide (LiBr), sodium carbonate (Na_2CO_3), sodium bicarbonate ($NaHCO_3$), anhydrous ethanol, urea, acetic acid, hydrogen peroxide (H_2O_2), sodium dodecyl sulfate (SDS) from Aladdin (Shanghai, China). Hydrochloric acid (HCl), sodium sulfate (Na_2SO_4), and glycerin were purchased from Sinopharm Chemical Reagent Co., LTD. (Shanghai, China). All chemicals were BR or AR grade. Unless otherwise stated, all reagents were commercially available and can be used without further purification.

Degreasing of Coarse Wool: The coarse wool was impregnated in 0.2 M sodium bicarbonate aqueous solution for 2 h with a wool-to-solution weight ratio of 1:20. After that, it was washed with deionized water and dried at 80 °C in a blast oven.

Extraction of Keratin Powder from Coarse Wool: The defatted wool was immersed in keratin solution (containing 10 wt.% Cys, 8 M urea, and 0.02 M SDS, pH = 11), sealed, and stirred at 90 °C for 4 h. The wool-to-keratin solution had a weight ratio of 1:20, preferably completely submerged wool. At the end of the dissolution process, the undissolved wool residue was removed by suction filtration to obtain a keratin solution. A mixed solution of 1 M Na_2SO_4 and 1 M HCl was drip-added to the keratin solution under constant stirring to reduce the solution pH below the isoelectric point of keratin, and the precipitated regenerated wool keratin was collected by filtration and thoroughly washed with deionized water. After that, the extraction rate of regenerated wool keratin powder was ≈79.9 ± 0.05 wt. % after freeze-drying, crushing, and sealing.

Preparation of Keratin Spinning Dope: The 25 wt. % extracted keratin powder, 13 wt. % DTT (based on keratin mass) and 10 wt. % SDS (based on keratin mass) were dissolved in 0.3 M Na_2CO_3/$NaHCO_3$ aqueous solution (pH = 9.5), and the spinning dope was stirred at room temperature for 24 h, then heated and stirred at 90 °C for 1 h. The transparent and viscous keratin spinning solution was prepared by centrifugation at 10 °C for 10 min.

Wet Spinning of Regenerated Wool Keratin Fiber (RWKF): Production of keratin fibers on continuous wet spinning lines (Figure S3, Supporting Information). The keratin dope in the syringe was extruded by a syringe pump at a flow rate of 0.2 mL min⁻¹ through a needle with an inner diameter of 310 µm and a length of 13 mm into a 10% v/v acetic acid and 10% v/v ethanol coagulation bath. Keratin filaments were drawn at v_1 into a 1% v/v hydrogen peroxide solution to ensure rapid reconstruction of disulfide bonds and at v_2 into a 1% v/v glycerol bath to improve the toughness of the keratin fiber and further remove impurities from the fiber surface. The fibers were subsequently dried through a drying oven and eventually rolled onto wooden spools.

Characterization: The rheological behavior of the keratin spinning dope was systematically characterized by the Rheometer DHR-2, and data were collected and analyzed using TRIOS v.4.4.1 software. The morphology of the prepared wool keratin fibers was characterized by FEI Quattro S scanning electron microscopy (SEM, Thermo Fisher Technology, USA). The thermal degradation stability of the fiber was tested by STA 449 F5 thermogravimetric analyzer (NETZSCH, Germany). Under nitrogen protection, the heating rate increased from 25 °C to 800 °C at 10 °C min⁻¹, and the gas consumption rate was set at 40 mL min⁻¹.

Attenuated total reflectance-Fourier transform infrared (ATR-FTIR) and Fourier Transform infrared (FTIR) spectra in the range of 4000–400 cm⁻¹ were recorded on an IRTracer-100 spectrometer (Shimadzu, Japan) to analyze functional groups of wool keratin fibers. The wool keratin powder and wet-spun fibers were characterized by X-ray diffraction (XRD) (Bruker D8 Advance diffractometer). Conventional copper target X-ray tube (λ = 1.54 Å), 40 kV, 40 mA, diffraction intensity recorded 2θ range 5°–40°, scanning speed of 0.05° s⁻¹. The crystallinity was calculated using Jade 6.0 software and Gaussian peak fitting was adopted. Raman spectroscopy (Raman) is recorded by a Raman microscope of Horiba LabRAM HR Evolution (Horiba, Japan) using a 633 nm excited laser. LabSpec software was used to collect and analyze Raman spectrum data. The Savitzky-Golay method was used for smoothing, denoising, and deconvolution in PeakFit v4.12 software. 2D SAXS/WAXS images of fibers were recorded on the Xeuss SAXS/WAXS system (XEUSS 3.0) of Shanghai synchrotron radiation source. The system used a Cu Kα (λ = 1.5418 Å) microfocus source and a Pilatus 300k detector in transmission mode in a vacuum. Data analysis and processing were performed using FOXTROT 3.4.9 software. Herman's factor (f) was calculated according to the following formula to evaluate the orientation of wool keratin fibers:

$$\cos^2\varphi = \frac{\int_0^{\frac{\pi}{2}} I(\varphi)\sin\varphi\cos^2\varphi\,d\varphi}{\int_0^{\frac{\pi}{2}} I(\varphi)\sin\varphi\,d\varphi} \tag{3}$$

$$f = \frac{1}{2}(3\cos^2\varphi - 1) \tag{4}$$

Mechanical Tests: Mechanical tests were performed according to ASTM D3822 standard, and samples were tested using EZ-LX electronic universal testing machine (Shimadzu, Japan) equipped with a 5 N sensor and pneumatic grip. Before the test, the fibers were balanced at standard conditions (21 °C, 65 RH %) for >48 h. The pulled keratin fibers were fixed on the cross-section table with conductive adhesive. The actual cross-section of each keratin fiber was recorded by SEM, and the accurate area was analyzed by Image J software.

Supporting Information

Supporting Information is available from the Wiley Online Library or from the author.

Acknowledgements

Conflict of Interest

The authors declare no conflict of interest.

Data Availability Statement

The data that support the findings of this study are available on request from the corresponding author. The data are not publicly available due to privacy or ethical restrictions.

[1] Z. Li, C. Chen, H. Xie, Y. Yao, X. Zhang, A. Brozena, J. Li, Y. Ding, X. Zhao, M. Hong, H. Qiao, L. M. Smith, X. Pan, R. Briber, S. Q. Shi, L. B. Hu, *Nat. Sustain.* **2022**, *5*, 235.

[2] Z. Y. Wang, X. Y. Qiao, K. Sun, *Carbohydr. Polym.* **2018**, *197*, 442.

[3] H. J. Lu, K. L. Xia, M. Q. Jian, X. P. Liang, Z. Yin, M. C. Zhang, H. M. Wang, H. M. Wang, S. Li, Y. Y. Zhang, *Research* **2022**, *2022*, 9854063.

[4] H. L. Xu, Z. Ma, Y. Q. Yang, *ACS Sustainable Chem. Eng.* **2014**, *2*, 1404.

[5] M. Zheng, K. R. Zhang, J. Zhang, L. L. Zhu, G. B. Du, R. B. Zheng, *Ind. Crops Prod.* **2022**, *188*, 115699.

[6] Y. J. Chen, Q. Zhang, Y. Zhong, P. D. Wei, X. J. Yu, J. C. Huang, J. Cai, *Adv. Funct. Mater.* **2021**, *31*, 2104368.

[7] S. H. Zhu, W. B. Zeng, Z. H. Meng, W. H. Luo, L. Y. Ma, Y. R. Li, C. X. Lin, Q. L. Huang, Y. H. Lin, X. Y. Liu, *Adv. Mater.* **2019**, *31*, 1900870.

[8] C. Y. Shi, J. L. Lan, J. J. Wang, S. Zhang, Y. H. Lin, S. H. Zhu, A. E. Stegmann, R. Yu, X. B. Yan, X. Y. Liu, *Adv. Funct. Mater.* **2020**, *30*, 2002882.

[9] L. Cera, G. M. Gonzalez, Q. Liu, S. Choi, C. O. Chantre, J. Lee, R. Gabardi, M. C. Choi, K. Shin, K. K. Parker, *Nat. Mater.* **2021**, *20*, 242.

[10] L. Zhang, F. Hu, S. H. Zhu, Y. H. Lin, Z. H. Meng, R. Yu, X. Y. Liu, *Small* **2020**, *16*, 2000128.

[11] S. I. N. Ayutthaya, S. Tanpichai, J. Wootthikanokkhan, *J. Polym. Environ.* **2015**, *23*, 506.

[12] Y. Ozaki, Y. Takagi, H. Mori, M. Hara, *Mater. Sci. Eng. C* **2014**, *42*, 146.

[13] A. Idris, V. Ranganathan, U. A. Rana, D. Fredericks, A. F. Patti, D. R. Macfarlane, *Green Chem.* **2013**, *15*, 525.

[14] K. Yamauchi, A. Yamauchi, T. Kusunoki, A. Kohda, Y. Konishi, *J. Biomed. Mater. Res.* **1996**, *31*, 439.

[15] FAOSTAT, *Production/Yield quantities of Shorn wool, greasy, including fleece-washed shorn wool in World*, https://www.fao.org/faostat/en/#data/QCL/visualize (accessed: December 2022.

[16] A. Shavandi, T. H. Silva, A. A. Bekhit, A. E. A. Bekhit, *Biomater. Sci.-UK* **2017**, *5*, 1699.

[17] C. Li, J. Liu, Y. Z. Chen, T. Li, X. X. Cai, J. Sung, X. S. Sun, *Chem. Eng. J.* **2018**, *336*, 54.

[18] K. Niinimäki, G. Peters, H. Dahlbo, P. Perry, T. Rissanen, A. Gwilt, *Nat. Rev. Earth Environ.* **2020**, *1*, 189.

[19] W. Zhao, R. Yang, Y. Zhang, L. Wu, *Green Chem.* **2012**, *14*, 3352.

[20] Y. Q. Zhang, W. Zhao, R. J. Yang, *ACS Sustainable Chem. Eng.* **2015**, *3*, 2036.

[21] E. Humes, *Nature* **2019**, *575*, 278.

[22] L. J. R. Nunes, R. Godina, J. C. O. Matias, J. P. S. Catalão, *J. Cleaner Prod.* **2018**, *171*, 1353.

[23] A. Helal, M. M. Mourad, *World Appl. Sci. J.* **2009**, *7*, 693.

[24] K. Wang, R. Li, J. H. Ma, Y. K. Jian, J. N. Che, *Green Chem.* **2016**, *18*, 476.

[25] B. Wang, Y. Wen, J. Mckittrick, M. A. Meyers, *Prog. Mater. Sci.* **2016**, *76*, 229.

[26] M. G. Yarrington, *Yale J. Biol. Med.* **1987**, *60*, 292.

[27] J. McKittrick, P. Y. Chen, S. G. Bodde, W. Yang, E. E. Novitskaya, M. A. Meyers, *JOM* **2012**, *64*, 449.

[28] X. T. Sun, X.i Wang, F. Q. Sun, M. W. Tian, L. J. Qu, P. Perry, H. Owens, X. Q. Liu, *Adv. Mater.* **2021**, *33*, 2105174.

[29] H. Xie, S. Li, S. Zhang, *Green Chem.* **2005**, *7*, 606.

[30] H. L. Xu, Y. Q. Yang, *ACS Sustainable Chem. Eng.* **2015**, *2*, 1404.

[31] H. Lundgren, A. Stein, *J. Phys. Chem. C* **1948**, *52*, 180.

[32] R. L. Wormell, F. Happey, *Nature* **1949**, *163*, 18.

[33] K. Katoh, M. Shibayama, T. Tanabe, K. Yamauchi, *J. Appl. Polym. Sci.* **2004**, *91*, 756.

[34] R. Liu, L. Li, S. Liu, S. Li, X. Zhu, M. Yi, X. Liao, *Adv. Polym. Technol.* **2018**, *37*, 2756.

[35] G. S. Cao, M. Z. Rong, M. Q. Zhang, *ACS Sustainable Chem. Eng.* **2020**, *8*, 18148.

[36] X. Mi, W. Li, H. L. Xu, B. N. Mu, Y. Chang, Y. Q. Yang, *Waste Manag* **2020**, *115*, 65.

[37] B. N. Mu, F. Hassana, Y. Q. Yang, *Green Chem.* **2020**, *22*, 1726.

[38] Z. Xia, Y. L. Shao, *Acta Phys.-Chim. Sin.* **2022**, *38*, 2103046.

[39] C. C. Chou, M. J. Buehler, *Biomacromolecules* **2012**, *13*, 3522.

[40] R. D. B. Fraser, T. P. Macrae, L. G. Sparrow, D. A. D. Parry, *Int. J. Biol. Macromol.* **1988**, *10*, 106.

[41] G. M. Gonzalez, J. Ward, J. Song, K. Swana, K. K. Parker, *Matter* **2020**, *3*, 742.

[42] D. Luo, S. W. Scott, B. D. Anderson, *J. Pharm. Sci.* **2005**, *94*, 304.

[43] M. Ghosh, B. P. Prajapati, N. Kango, K. K. Dey, *Solid State Nucl. Magn. Reson.* **2019**, *101*, 1.

[44] Z. L. Zhang, Y. Nie, Q. S. Zhang, X. Liu, W. H. Tu, X. P. Zhang, S. J. Zhang, *ACS Sustainable Chem. Eng.* **2017**, *5*, 2614.

[45] C. Gaidau, D. Epure, C. E. Enascuta, C. Carsote, C. Sendrea, N. Proietti, W. Y. Chen, H. B. Gu, *J. Clean. Prod.* **2019**, *236*, 117586.

[46] M. J. Duer, N. McDougal, R. C. Murray, *Phys. Chem. Chem. Phys.* **2003**, *5*, 2894.

[47] R. Paquin, P. Colomban, *J. R. Spectrosc.* **2007**, *38*, 504.

[48] A. Kuzuhara, *Biopolymers* **2005**, *77*, 335.

[49] A. Kuzuhara, T. Hori, *Biopolymers* **2005**, *79*, 324.

[50] A. Kuzuhara, T. Hori, *Biopolymers* **2006**, *81*, 506.

[51] H. Tu, R. Yu, Z. F. Lin, L. Zhang, N. B. Lin, W. D. Yu, X. Y. Liu, *Adv. Funct. Mater.* **2016**, *26*, 9032.

[52] J. L. Kong, S. N. Yu, *Acta Biochim. Biophys. Sin.* **2007**, *39*, 549.

[53] S. Feroz, N. Muhammad, J. Ranayake, G. Dias, *Bioact. Mater.* **2020**, *5*, 496.

[54] G. S. Cao, Z. P. Zhang, M. Z. Rong, M. Q. Zhang, *SusMat.* **2022**, *2*, 90.

[55] A. J. Poole, J. S. Church, M. G. Huson, *Biomacromolecules* **2009**, *10*, 1.